European Journal of Biotechnology and Bioscience

www.biosciencejournals.com

E J B B

European Journal of Biotechnology and Bioscience

ISSN: 2321-9122
www.biosciencejournals.com
EJBB 2014; 2 (6): 30-46
Received: 06-12-2014
Accepted: 24-12-2014

Syed Hussain Basha
Innovative Informatica Technologies, 3-201, HIG, Lane Opposite Lakshmi SBI Homes, HUDA, Mayuri Nagar, Miyapur, Hyderabad – 500 049, India.

Prakash Bethapudi
Department of CSE, GITAM University – 530 045, Visakhapatnam, Andhra Pradesh, India.

Majji Rambabu
Innovative Informatica Technologies, 3-201, HIG, Lane Opposite Lakshmi SBI Homes, HUDA, Mayuri Nagar, Miyapur, Hyderabad – 500 049, India.

Firoz. A
Center for Genetics and Inherited Diseases, College of Medicine, Taibah University, PO Box 3001, Medina, Saudi Arabia.

N.V.S. Viswanadha murty M
Department of Pharmaceutical chemistry, A.U. College of Pharmaceutical Sciences, Andhra University – 530 003, Visakhapatnam, Andhra Pradesh, India.

Sreenivasa reddy E
Department of CSE, Acharya Nagarjuna University – 522 510, Guntur, Andhra Pradesh, India.

Correspondence:
Syed Hussain Basha
Innovative Informatica Technologies, 3-201, HIG, Lane Opposite Lakshmi SBI Homes, HUDA, Mayuri Nagar, Miyapur, Hyderabad – 500 049, India.

Anti-angiogenesis property by Quercetin compound targeting VEGFR2 elucidated in a computational approach

Syed Hussain Basha, Prakash Bethapudi, Majji Rambabu, Firoz. A, N.V.S. Viswanadha murty M, Sreenivasa reddy E

Abstract
Quercetin is a naturally occurring flavonoid compound found in various species of vegetables and fruits**.** This compound have been widely demonstrated for having various medicinal properties including its capacity to inhibit enzymes that activate carcinogens, anti-viral, antioxidative activity as well as to modify signal transduction pathways by interacting with regulatory cell receptors etc., On the other hand, recent reports have evidenced significant anti-angiogenesis property of this compound on rat models targeting VEGFR2 regulated signalling pathways. In this scenario, we have carried out this present study to elucidate the underlying interactions responsible for this strong target specific inhibition at the molecular level using different computational approaches. Our docking, binding free energy along with molecular dynamic simulation studies revealed various interactions responsible for this target specific binding involving large negative binding energies. Quercetin compound demonstrated out ruling properties and interactions when compared the results with the VEGFR2 co-crystallized ligand AAZ. The present results would be of high value for further designing potent target specific anti-angiogenesis drug compounds.

Keywords: Quercetin, VEGFR2, docking, Molecular dynamic simulations, anti-angiogenesis.

1. Introduction
Cancer is a group of various diseases all of which are involved in rapid division of cells leading to uncontrolled cell growth. There are about 200 different types of cancers known, which are classified based on the type of cells that could affect. Cancer can develop in almost any organ or tissue, such as the lung, colon, breast, skin, bones, or nerve tissue. The cancer is known to spread through lymphatic system or blood stream to all over the body [1]. Many things increase the complexity of the cancer by causing damage at gene level, including tobacco usage, infections, radiations, lack of physical activity and environmental pollutants [2].
As per GLOBOCAN review, in 2012 itself 14.1 million new cancer cases were reported and about 8.2 million cancer-related deaths occurred. Worldwide there are about 1.8 million (13.0%) lung cancer, 1.7 million (11.9%) breast cancer, and 1.4 million (9.7%) colorectal cancer types have been diagnosed. The most common causes of cancer death were reported with lung cancer 1.6 million, (19.4%), liver 0.8 million (9.1%) and stomach 0.7 million (8.8%). It was estimated that there will be a gradual increase of 19.3 million new cancer cases per year by 2025. Breast cancer is the most frequently diagnosed cancer type among women; 12.7 million women were diagnosed with breast cancer and 5, 22, 000 deaths were recorded in the year 2012 [3]. Hence, finding potent drug candidates against cancer is of primary urgency. Since, there are various types of cancers present; it is an important strategy to choose a mechanism in common to inhibit all types of cancers.
For any type of cancer to spread, new blood vessel formation is crucial for transportation of vital nutrition for the tumour growth and survival. The process of creating new blood vessels from pre-existing blood vessels is known as Angiogenesis. It involves a complex process of activation, proliferation and migration of endothelial cells to form new capillaries. This complete mechanism of angiogenesis can be found most extensively in the process of wound healing and the formation of placenta during embryonic development stage of pregnancy [4-8].

2. Role of VEGFR2 in angiogenesis

At molecular level, various signalling pathways such as AKT/mTOR/P70S6K pathways induce angiogenesis. Activation of this signalling pathways involved in angiogenesis is reported to be because of Vascular Endothelial Growth Factor A (VEGF-A) binding with the extra cellular domain of Vascular endothelial growth factor receptor 2 (VEGFR2) resulting for its auto-phosphorylation. Thus, inhibition of this VEGF-A binding with VEGFR2 is an attractive drug target for biological cancer therapies, moreover there is demonstrated evidence that inhibition of VEGFR2 not only blocks angiogenesis in tumors but can also destroy tumor vessels [9], hence it is considered as a validated drug target for angiogenesis [10]. Cabozantinib [11] 5-(Ethylsulfonyl)-2-methoxyaniline (5)-aaz [12]; Taxifolin [13]; Decursin [14] and Bevacizumab [15] are few of the FDA approved compounds presently available in the market as anti-angiogenesis drugs targeting VEGFR2. Structurally, VEGFR2 contains the kinase core along with 18 residues from kinase insert domain. TYR 1054 and TYR1059 residues present at the kinase activation loop of VEGFR2 is proven to be its autophosphorylation site [16]. Whereas, GLU883; VAL 914; GLU 915; PHE916; CYS917; ASN921 ASP1044 and PHE 1045 residues were reported to be the crucial role players towards forming strong receptor-ligand binding via hydrogen bonds and pi-pi stackings [17-18].

3. Anti-angiogensis property by Quercetin

Quercetin is naturally occurring flavonoid compound found in about 28 different vegetables and nine fruits varieties such as apples, tea (Camelia sinensis), red onions, capers, lovage, parsley, broccoli, berries and red grapes [19-20]. This flavonoid compound have been reported to be having various medicinal properties including its capacity to inhibit enzymes that activate carcinogens, anti-viral, antioxidative activity as well as to modify signal transduction pathways by interacting with regulatory cell receptors and other proteins [21-22].

Recently, Quercetin compound at 20mg/kg/d dosage was shown to be having significant anti-angiogenesis effect in ex vivo, in vivo and in vitro rat models. It was demonstrated that this compound suppress the VEGF induced phosphorylation of VEGFR2 and their downstream protein kinases mOTR, AKT, and ribosomal protein S6 kinase. On the other hand, significant reduction in solid tumour weight in prostate xenograft mouse models was observed, indicating this compound's potential to act as anti-angiogenesis drug compound [23]. Based on this recent evidence it was clear that Quercetin could be used as a potential drug candidate for cancer therapy targeting VEGFR2 regulated signalling pathways. In this scenario, keeping in view of the increased applications and reliability on computational methods towards discovering novel drug candidates for reducing time and cost, we have carried out this present study to elucidate the underlying interactions responsible for this strong target specific inhibition at molecular level using different computational approaches. The knowledge thus gained could of high value in designing novel anti-angiogenesis drug candidates targeting VEGFR2.

4. Computational Methods

4.1 Preparation of protein structure

Crystal structure of VEGFR2 in complex with 2-anilino-5-aryl-oxazole (AAZ) [PDB ID: 1Y6A] [24] which was resolved using X-Ray diffraction method with a resolution factor of 2.30 Å was retrieved from Protein Data Bank (*www.rcsb.org*) [25]. Retrieved structure has been further modified for Glide docking calculations as follows: For Glide v6.1 [26-29] calculations, VEGFR2-2-anilino-5-aryl-oxazole complex was imported to Maestro v9.6 [30]. Using Protein Preparation Wizard (PPW) [31-32], included Biological unit and assigned bond orders, created zero order bonds to metals, created disulfide bonds, converted any selenomethionines to methionines, deleted all water molecules, generated metal binding states, added missing hydrogens, filled any missing side chains and missing loops and capped the termini making use of the prime module integrated within PPW. Under review and modify tab of PPW, all the co-crystallized ligands/hetero atoms and waters were detected and removed from the structure. Under the refine tab of PPW, we have optimized the H-bond network to fix the overlapping hydrogens and the most likely positions of thiol and hydroxyl hydrogen atoms. Protonation states and tautomers of 'His' residues, and Chi 'flip' assignments for 'Gln', 'Asn' and 'His' residues were selected by the protein assignment script shipped by Schrodinger. pH range was set to 7.0 and the protein was minimized by applying OPLS2005 force field [33-34]. Finally, restrained minimization was performed until the average root mean square deviation (RMSD) of the non-hydrogen atoms converged to 0.30 Å. Glide's grid generation module has been used to represent the shape and properties of the receptor by different sets of fields that provide progressively more accurate scoring of the ligand poses.

4.2 Preparation of ligands

The three dimensional coordinates of AAZ (CID 4369497) and quercetin compounds (CID 5280343) were retrieved from Pubchem database (*http://pubchem.ncbi.nlm.nih.gov/*). Structures of these two compounds used in the present study are shown in Figure 1.

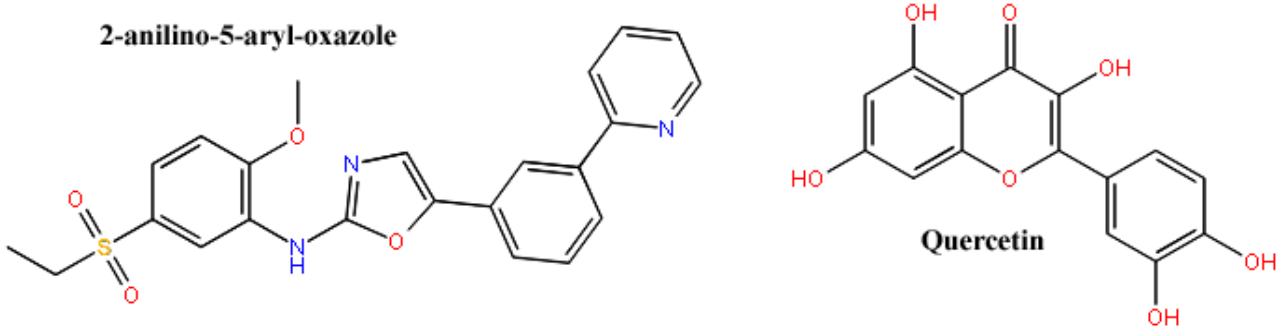

Fig 1: Structures of 2-anilino-5-aryl-oxazole and Quercetin compounds.

Using LigPrep Ver 2.8 module [35] of the Schrodinger suite 2013.3, each structure was minimized using OPLS_2005 force field and Ionization states was set to generate all possible states at pH 7.0 +/- 2.0 and metal binding states to the compounds were generated and retained the original states for the given ligand using "EpiK". Ligands were desalted and allowed to generate tautomers. Under the stereoisomer's column we have specified to retain chiralities and allowed to generate 32 per ligand at most. Keeping in view of the flexibility of the rings present in each ligand and their possibility to change conformations during docking calculations, we have specified to generate low energy ring conformation with 1 per ligand.

4.3 Ligand docking

GLIDE (Grid-based Ligand Docking with Energetics) v6.1 module in Schrodinger software was used for all the docking calculations. It uses a grid based ligand docking method with energetic and searches for favourable interactions between one or more small ligand molecules and receptor protein. Once, it has been ensured that the protein and ligands are prepared for docking; a receptor grid file was generated using grid receptor generation program available with Glide module. In order to keep the protein receptor flexible, we have allowed the rotation of hydroxyl and thiol groups of THR862; CYS917; THR925; TYR1006; SER1035; CYS1043; ASH1044 residues. A grid box of size 80 x 80 x 80 Å with coordinates X = 0.35, Y = 29.8 and Z = 17.8 was generated and the size of ligands to be docked was selected as no more than 20 Å. The ligands were docked with the active site using the 'extra precision' Glide algorithm.

4.4 ADME screening

The QikProp ver.3.8 program [36] integrated within Schrodinger was used to obtain the ADME properties of the tested compounds. It predicts both physically significant descriptors and pharmaceutically relevant properties. The program was processed in normal mode with neutralized ligand input and allowed it to predict 35 principal and physiochemical properties for the given compound. Among the predicted descriptors, molecular weight, H-bond donors, H-bond acceptors, log P (Octanol/water), log P MDCK, log Kp (skin permeability), humoral absorption are few important ones. It also evaluates the CNS activity and Blood brain barrier crossing ability of the compounds along with acceptability of the ligands for drug like molecules based on Lipinski's rule of 5 [37]. Lipinski's rule of 5 is proven to be reliable criteria to evaluate drug likeness, or determine if a chemical compound with a certain pharmacological or biological activity has properties that would make it a likely orally active drug in humans. The rule describes molecular properties important for a drug's pharmacokinetics in the human body, including its ADME.

4.5 MM-GBSA/Prime binding-free energy calculation

GLIDE XP docking output pose viewer file was used to calculate the binding free energies of protein-ligand complex using OPLS-AA force field and GB/SA continuum solvent model incorporated in Prime/MM-GBSA protocol [38-39].

4.6 MD Simulations in water

''Desmond v3.6 Package'' [40-42] was used to run the molecular dynamic simulations. Predefined TIP3P water model [43] was used to simulate water molecules using OPLS2005 force field. Orthorhombic periodic boundary conditions were set up to specify the shape and size of the repeating unit buffered at 10 Å distances. In order to neutralize the system electrically, appropriate counter NA+/Cl- ions were added to balance the system charge and were placed randomly in the solvated system. After building the solvated system, we have performed minimization and relaxation of the protein/protein-ligand complex using default protocol of desmond; which includes a total of 9 stages among which there are 2 minimization and 4 short simulations (equilibration phase) steps are involved before starting the actual production time.

Summary of Desmond's MD simulation stages:

stage 1 – task (recognizing the simulation setup parameters)
stage 2 - minimize, Minimization with restraints on solute
stage 3 - minimize, Minimization without any restraints
stage 4 - simulate, Berendsen NVT, T = 10 K, small timesteps, and restraints on solute
heavy atoms
stage 5 – simulate, Berendsen NPT, T = 10 K, and restraints on solute heavy atoms
stage 6 - solvate_pocket
stage 7 – simulate, Berendsen NPT and restraints on solute heavy atoms
stage 8 – simulate, Berendsen NPT and no restraints
stage 9 – simulate (production time)

Molecular dynamic simulations were carried out with the periodic boundary conditions in the NPT ensemble [44] using OPLS 2005 force field parameters. The temperature and pressure were kept at 300 K and 1 atmospheric pressure using Nose-Hoover temperature coupling and isotropic scaling [45], the operation was followed by running the 5 ns NPT production simulation and saving the configurations thus obtained at 5ps intervals. All the Glide dockings and molecular dynamic simulations were performed on Intel (R) Core (TM) i5-3330 Processor CPU @ 3.00 GHz with 8 GB DDR RAM. Schrödinger software was compiled and run under Linux CentOS 6.4 (Final) operating system. All the Glide docking and Molecular dynamics simulation snapshots were rendered using Schrodinger's maestro interface v9.6.

5. Results and Discussion

5.1 Molecular Docking:

In order to study the detailed molecular basis of interactions and binding affinity of the ligands comparatively with VEGFR2 active site. Prepared structures of 2-anilino-5-aryl-oxazole (co-crystallized compound with VEGFR2) along with Quercetin compound were docked into the active site of VEGFR2. The docking results of the ligand are given in table 1.

Table 1: Docking energies and interaction profile of 2-anilino-5-aryl-oxazole (VEGFR2 co-crystallized ligand found in PDB 1Y6A) and Quercetin compound with VEGFR2:

S.No	Ligand name	Pubchem ID	XP GLIDE score	Interactions	
				H-bond	Hydrophobic
1.	2-anilino-5-aryl-oxazole	4369497	-8.9	ILE1042, LEU1034	LEU1017, MET1014, CYS1043, LEU838, PRO837, ILE1032, LEU1033, VAL896, PHE1086, VAL897, VAL1040, VAL914, VAL865, ILE847 , CYS917, LEU1034, PHE919
2.	Quercetin	5280343	-9.1	LEU1033	PHE916,LEU1033, LEU1034, PHE919, CYS917, ALA864, ILE1042, VAL914, PHE1016,VAL897, LEU1017, VAL845, PHE1045, CYS1043, ILE1032, LEU838,

The results of docking simulations demonstrated high binding affinity with promising interactions with catalytically important residues present at the VEGFR2's active site with binding energies of -8.9 and -9.1 Kcal/mol for 2-anilino-5-aryl-oxazole and Quercetin compounds respectively. The high binding affinity of quercitin compound towards VEGFR2 in comparison to 2-anilino-5-aryl-oxazole has evidenced its potent inhibiting capability.

When the docked complexes were analyzed for the interactions involved, it was observed that 2-anilino-5-aryl-oxazole was shown to be forming direct hydrogen bonds with ILE1042 and LEU1034 along with hydrophobic interactions with LEU1017, MET1014, CYS1043, LEU838, PRO837, ILE1032, LEU1033, VAL896, PHE1086, VAL897, VAL1040, VAL914, VAL865, ILE847, CYS917, LEU1034 and PHE919 residues of VEGFR2 (Figure 2).

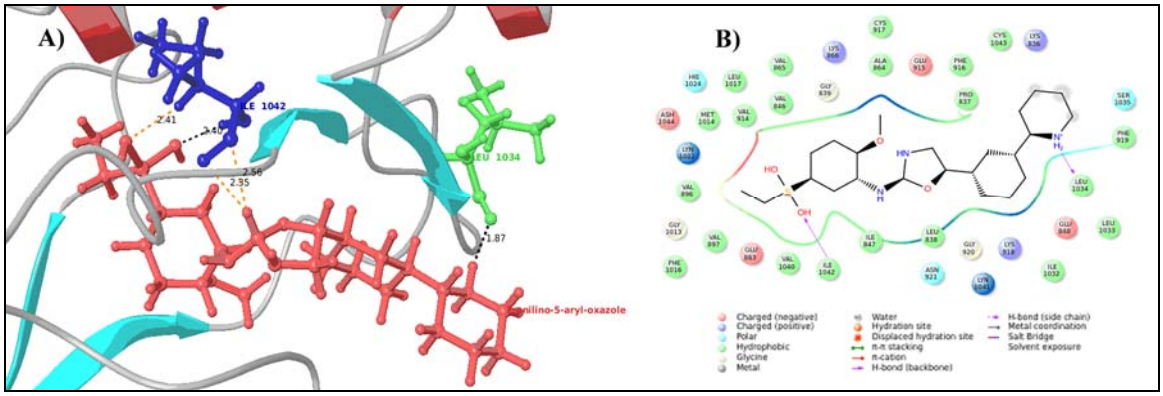

Fig 2: Docking snapshot of VEGFR2 in complex with 2-anilino-5-aryl-oxazole:: a) Showing H-bond and contacts formed by AAZ with VEGFR2 residues LEU 1034 and ILE 1042 b) 2D interactions snapshot showing various interactions formed by AAZ at the catalytic active site of VEGFR2.

When the docking snapshot of Quercetin in complex with VEGFR2 was analysed, Quercetin compound was shown to be forming a direct hydrogen bond with LEU1033 residue, along with hydrophobic interactions with PHE916, LEU1033, LEU1034, PHE919, CYS917, ALA864, ILE1042, VAL914, PHE1016, VAL897, LEU1017, VAL845, PHE1045, CYS1043, ILE1032 and LEU838 (Figure 3).

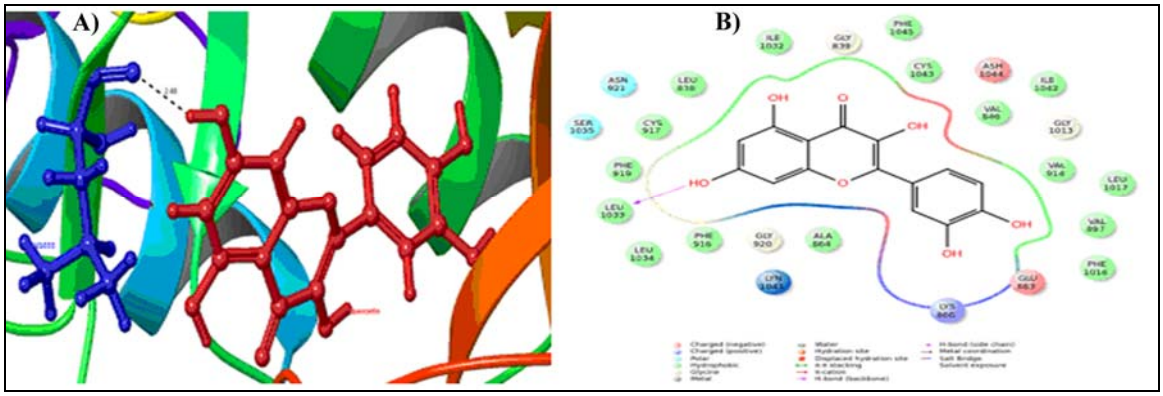

Fig 3: Docking simulation snapshot of VEGFR2 in complex with QUERCETIN: a) Showing H-bond and contacts formed by Quercetin with VEGFR2 residues LEU1033 b) 2D interactions snapshot showing various interactions formed by Quercetin at the catalytical active site of VEGFR2.

On the other hand, ADME predictions by Qikprop program have shown to be having significantly promising ADME properties which are well within permissible range (Supplementary table 1).

5.2 MM-GBSA/Prime binding-free energy analysis

We have applied binding free energy analysis approach in order to further validate the docking energy predictions, for the receptor and ligand complex, since the exclusivity of the

scoring functions used in docking program is not fully reliable [46]. VEGFR2-Quercetin complex predicted to be having binding free energy of -54.245 Kcal/mol, whereas VEGFR-2-AAZ complex was predicted to be having -33.14 Kcal/mol. This results further validates and evidences high binding affinity along with thermodynamic stability of VEGFR2-Quercetin complex in comparison to VEGFR2-AAZ complex.

5.3 MD Simulations

We have performed molecular dynamic simulations in order to study the protein-ligand interactions in motion contributing for their thermodynamic stability and to visualize the effect of ligand binding on protein conformational changes. For better understanding and comparison, firstly we have subjected the protein VEGFR2 (without any ligand) to MD simulations, then after VEGFR2 in complex with AAZ (co-crystallized ligand with VEGFR2) and finally VEGFR2 in complex with Quercetin. Statistically significant comparative results have been presented in Table 2 and overall stability of the simulated system was demonstrated via simulation quality analysis report, results of which have been presented in Supplementary table 2.

Table 2: MD trajectory analysis of VEGFR2 without any ligand and in complex with QUERCETIN:

S.No	Molecule	Statistical Parameter									
		Total energy (Kcal/mol)		RMSD (Backbone)		Radius of gyration		Intra molecular H-Bonds		Inter molecular H-Bonds	
		Range	Mean	Range	Mean	Range	Mean	Range	Mean	Range	Mean
1.	VEGFR2 (without any ligand)	-5.6 to -4.8	-5.2	0.0 to 2.8	2.3	20.2 to 20.9	20.6	106 to 142	121	N/A	N/A
2.	VEGFR2 in complex with AAZ	-3.7 to -3.0	-3.3	0.0 to 2.7	2.0	20.3 to 21.0	20.6	66 to 92	80	0.0 to 5.0	3.1
3.	VEGFR2 in complex with quercetin	-5.6 to -4.8	-5.3	0.0 TO 5.2	3.9	20.5 to 21.2	20.9	108 to 140	123	1.0 to 6.0	3.4

To analyze the stability and overall conformational changes of VEGFR2 protein receptor comparatively, we have studied the total energy [Figure 4], Root mean square deviation (RMSD) [Figure 5], Radius of gyration (ROG) [Figure 6], Root mean square fluctuations (RMSF) [Figure 7]; total intra molecular hydrogen bonds [Figure 8] and total secondary structure elements (SSE) [Figure 9] contributions as the time dependant function of MD simulations. We have analyzed the total energy involved for the stabilized conformation of this protein, it was observed to be having an average of -5.2 Kcal/mol of energy in a range of –5.6 to -4.8 Kcal/mol for apo protein (figure 4a); -3.3 Kcal/mol of energy in a range of -3.8 to -3.0 kcal/mol for VEGFR2-AAZ complex (figure 4b) and an average -5.3 Kcal/mol of energy in a range of -5.7 to -4.8 Kcal/mol for VEGFR2-Quercetin complex (figure 4c), which clearly demonstrates the comparative high binding affinity of Quercetin compound in comparison to AAZ, this much minimized negative energy further substantiates high thermodynamic stability of this complex in comparison along with its inhibitory potential.

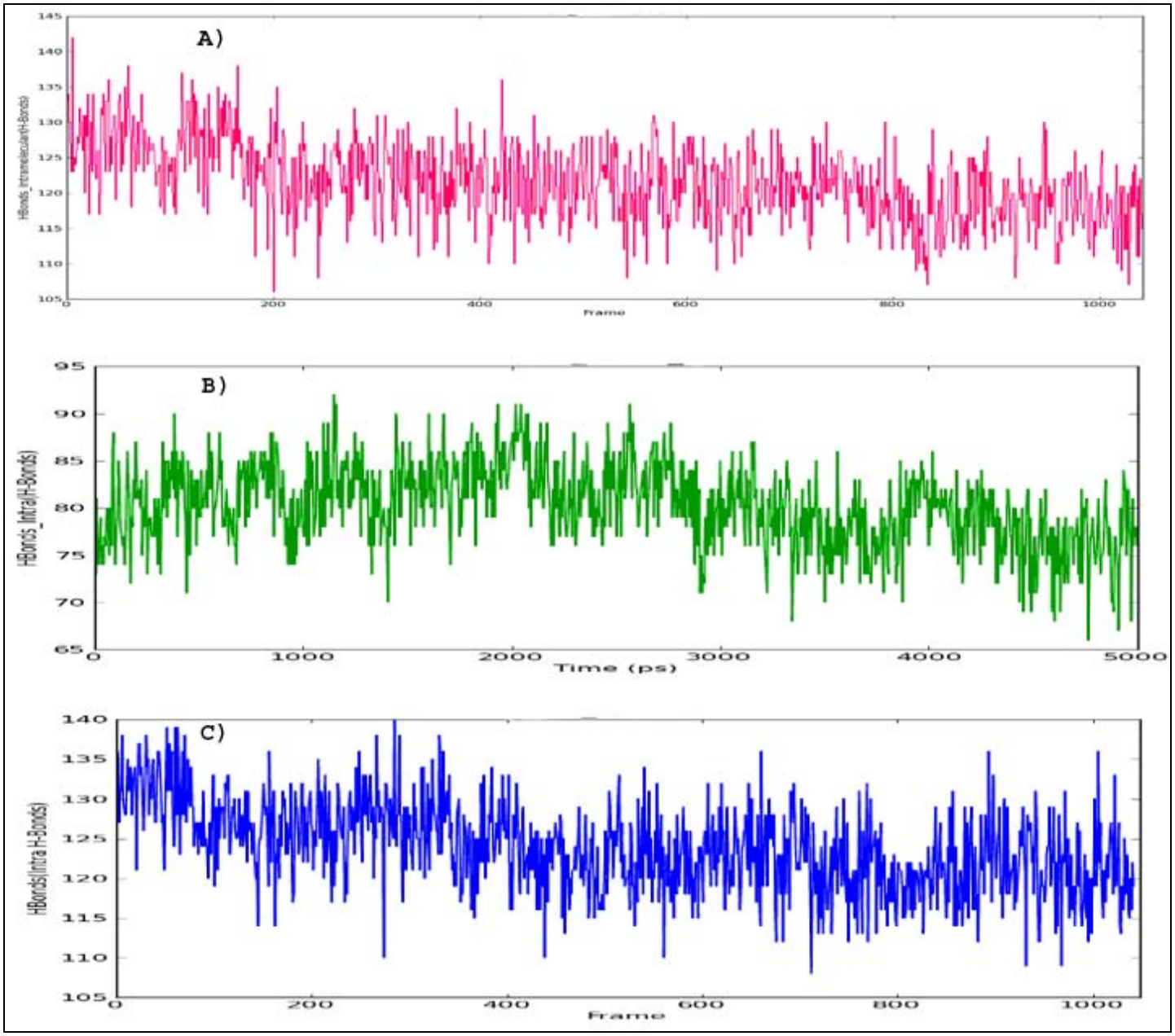

Fig 4: Analysis of total energy of the VEGFR2 protein in its A) Apo state (red); B) in complex with AAZ (green) and C) in complex with Quercetin compound (blue) during simulated time.

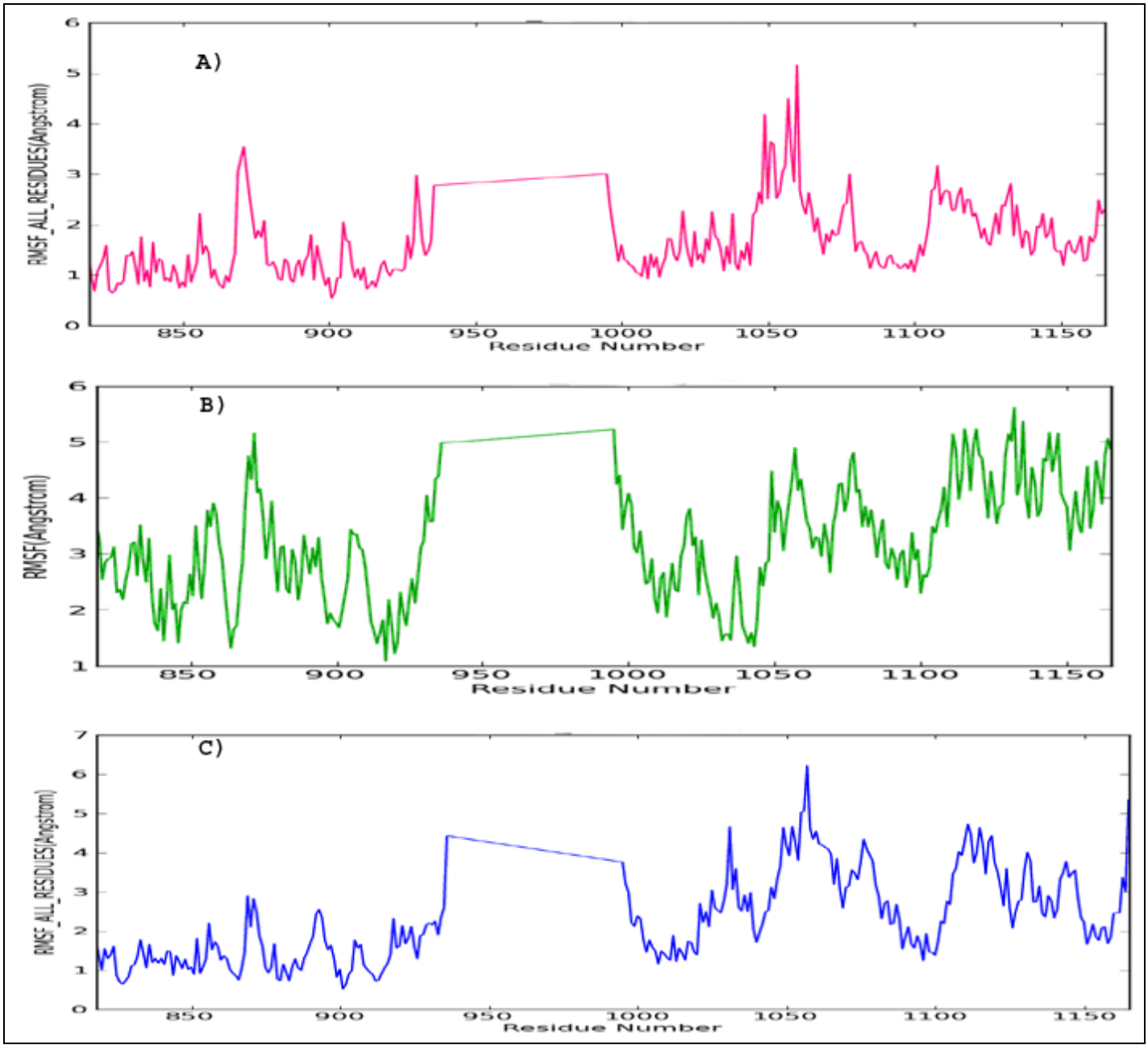

Fig 5: Analysis of Root mean square deviations (RMSD) of the VEGFR2 protein in its A) apo state; B) in complex with AAZ and C) in complex with Quercetin compound during simulated time.

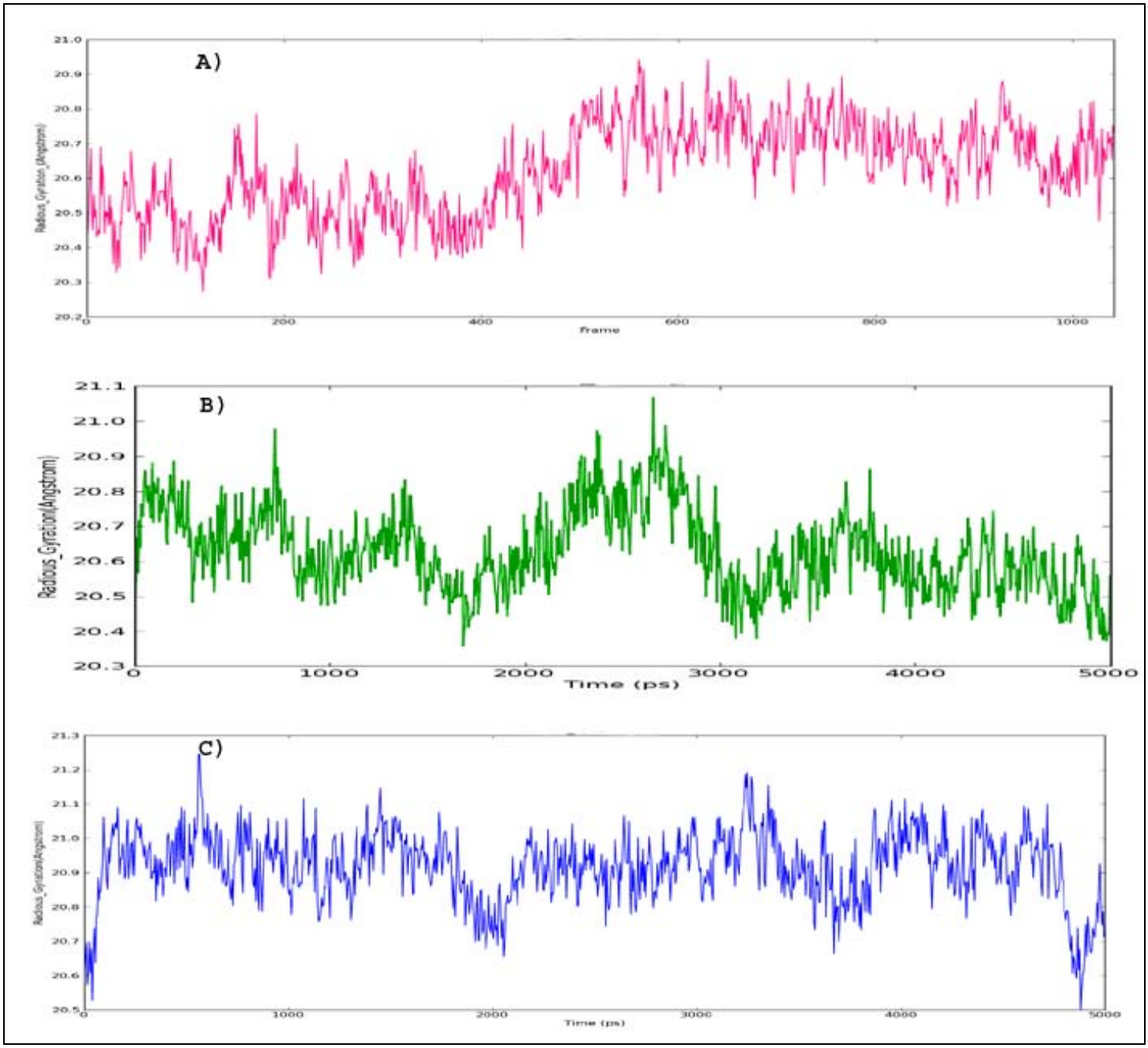

Fig 6: Analysis of radius of gyration of the VEGFR2 protein in its A) apo state (red); B) in complex with AAZ (green) and C) in complex with Quercetin compound (blue) during simulated time.

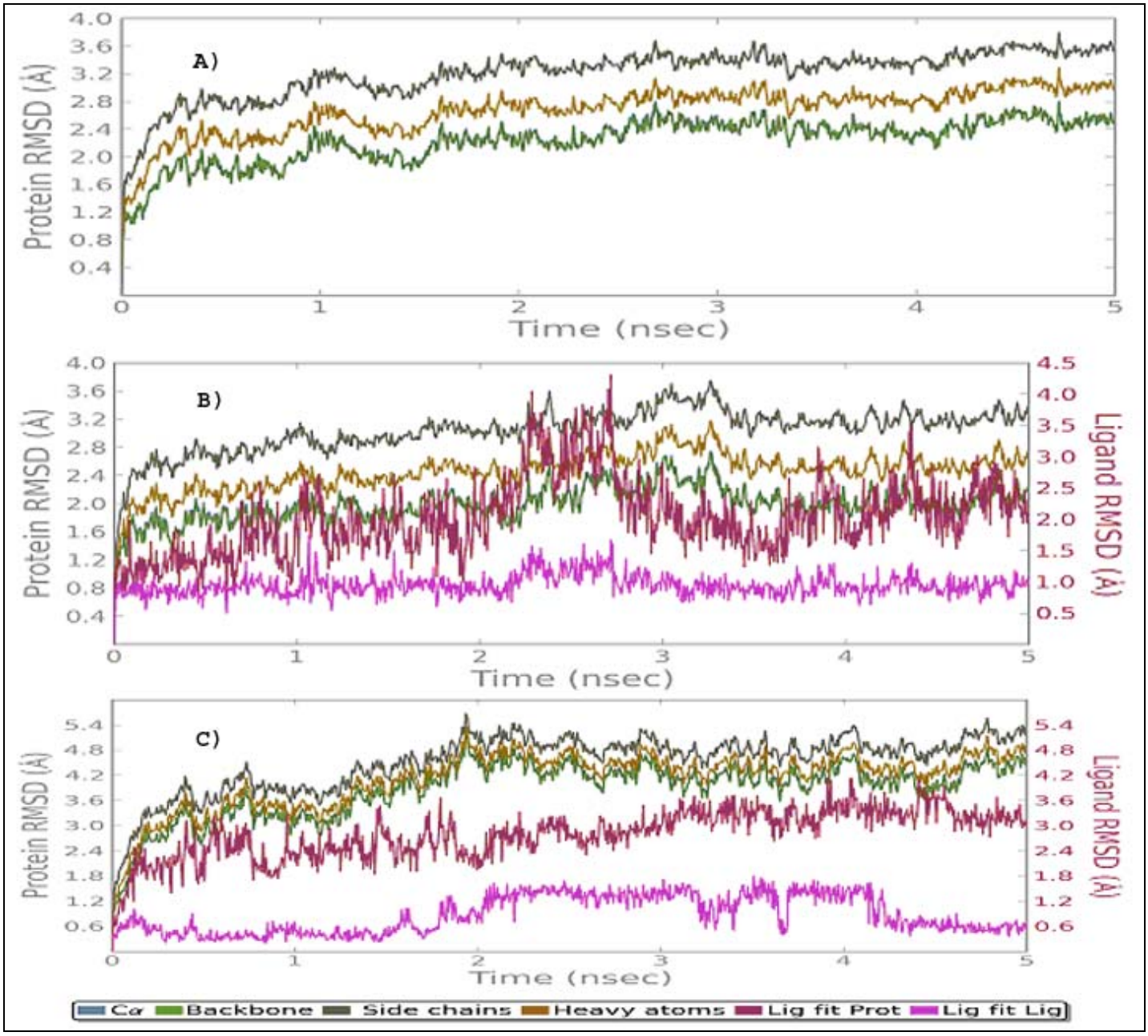

Fig 7: Analysis of Root mean square fluctuations (RMSF) of the residues present in VEGFR2 protein in its A) apo state (red); B) in complex with AAZ (green) and C) in complex with Quercetin compound (blue) during simulated time.

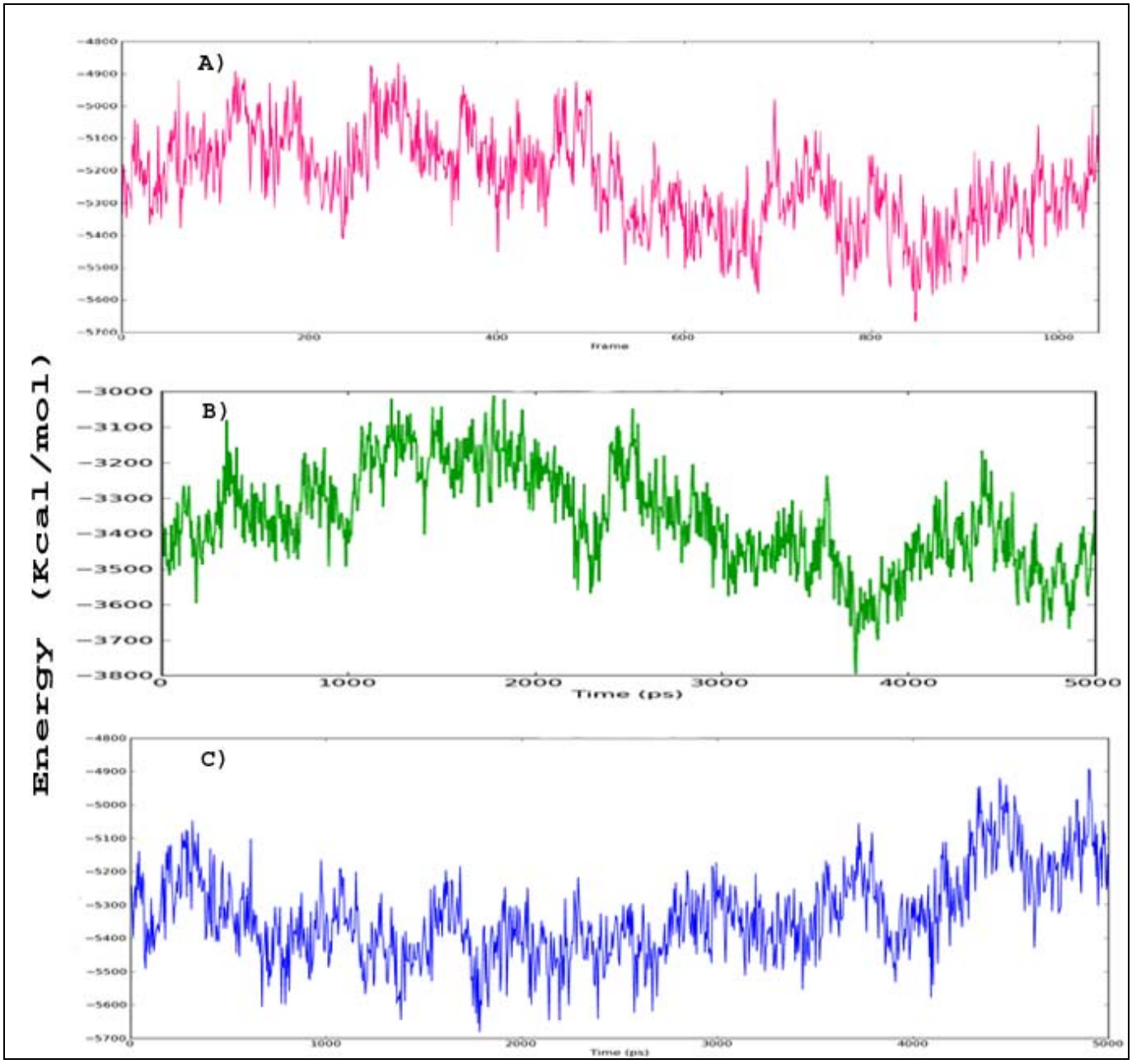

Fig 8: Analysis of total intra molecular hydrogen bonds present in VEGFR2 protein in its A) apo state (red); B) in complex with AAZ (green) and C) in complex with Quercetin compound (blue) during simulated time.

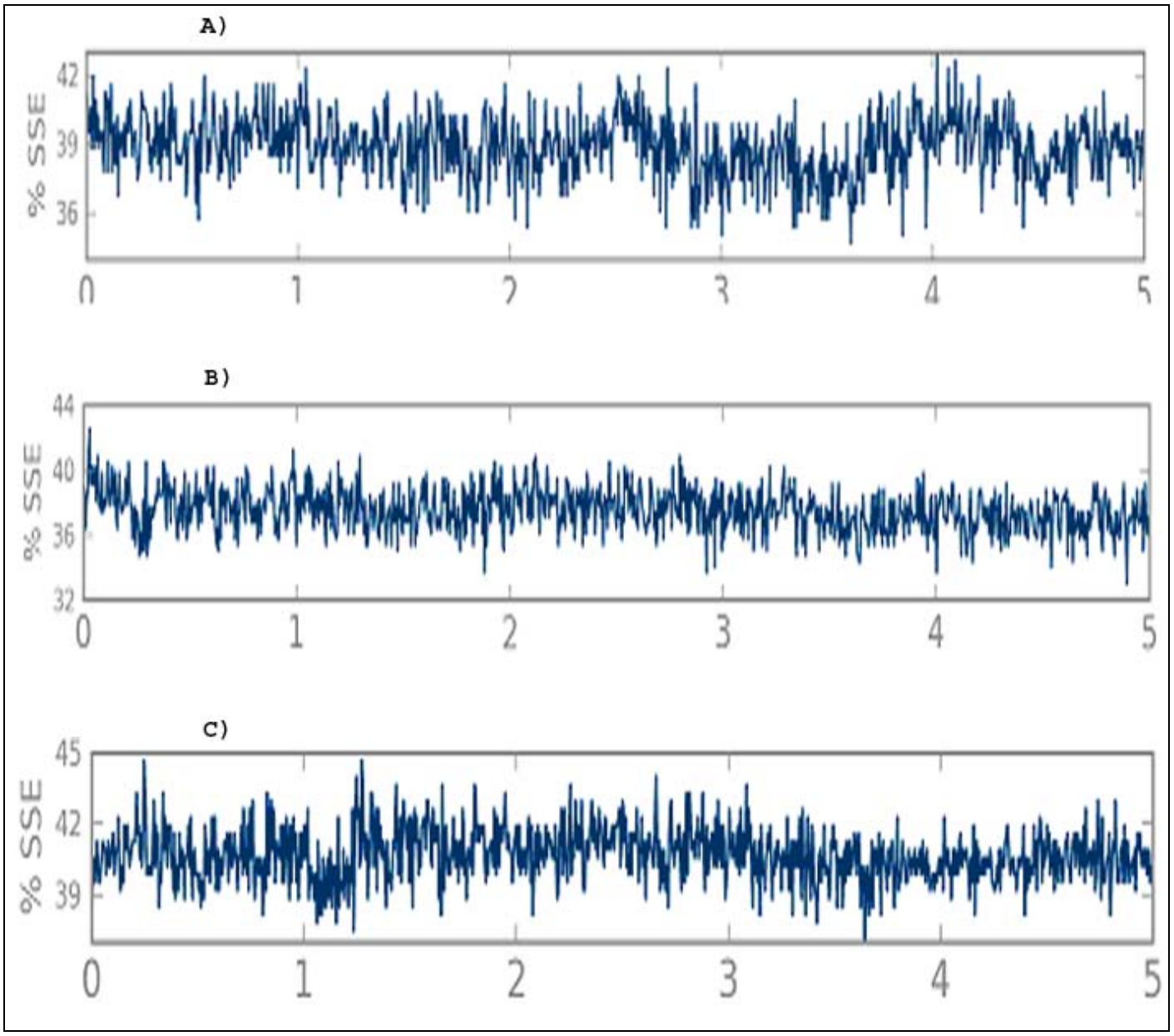

Fig 9: Analysis of Secondary structure elements (SSE) percentage like alpha helices and beta strands present in VEGFR2 in its A) apo state B) in complex with AAZ and C) in complex with Quercetin compounds during the simulation trajectory.

In order to understand the conformational changes in the overall protein in its apo state and in presence of the given ligands, RMSD of the protein's c-alpha chain, backbone, side chains and heavy atoms present in the protein has been analyzed along with the RMSD of ligand with reference to the protein as well as with reference to the docked ligand conformation. When the RMSD of the protein VEGFR2 in its apo state was analyzed, its c-alpha chain and backbone found to be fluctuating around 2.4 Å, where as the side chains and heavy atoms were shown to be fluctuating around 3.6 Å and 2.8 Å respectively (figure 5a). Further, we have calculated RMSDs for the trajectory of VEGFR2 in complex with AAZ using its initial model as a reference structure. The results in figure 5b show that the RMSDs of the trajectory for the complex shows that the c-alpha chain and backbone are fluctuating around 2.0 Å, where as the side chains and heavy atoms were shown to be fluctuating around 3.6 Å and 2.4 Å respectively. We have also analyzed the ligand AAZ's RMSD with reference to the protein (ligand fit to protein) as well as with reference to its docked conformation (ligand fit ligand). The results shows that the ligand fit to protein RMSD is fluctuating around 2.5 Å, with few high peaks upto 4.0 Å in between 2-3ns of simulated chemical time, whereas ligand fit ligand RMSD showed a steady graph maintaining at 1.0 Å. Finally, we have analyzed the RMSDs for the trajectory of VEGFR2 in complex with Quercetin. The results in figure 5c show that the RMSDs of the trajectory for the complex shows that the c-alpha chain and backbone are fluctuating around 4.8 Å, whereas the side chains and heavy atoms were shown to be fluctuating around 5.4 Å and 4.9 Å respectively. We have also analyzed the ligand Quercetins' RMSD with reference to the protein (ligand fit to protein) as well as with reference to its docked conformation (ligand fit ligand). The results shows that the ligand fit to protein RMSD is fluctuating around 3.0 Å, whereas ligand fit ligand RMSD shown to be maintaining an average of around 0.6 Å.

In order to estimate the overall compactness of the protein structure, we have calculated the radius of gyration (ROG) during the simulated time (figure 6). Throughout the simulation time, VEGFR2 protein was measured to be

having a ROG in a range of 20.2 Å to 20.9 Å with an average of 20.6 Å for apo protein; 20.3 Å to 21.1 Å with an average of 20.7 Å for VEGFR2 in complex with AAZ and 20.5 Å to 21.3 Å with an average of 21.0 Å for VEGFR2 in complex with Quercetin compound (table 2). With this ROG data we can say that the protein is quite stable, however, as the simulation progresses, protein was found to be expanding a bit in its overall structure in its apo state after passing half of the simulation time, in contrary VEGFR2 in complex with AAZ compound shows that the protein compactness is fluctuating comparatively and found to be contracting at the last 3 ns of the simulated time. Whereas, in case of VEGFR2 in complex with Quercetin, the overall protein was found to be expanding compared to ROG data of apo protein.

To identify the actively moving residues during the simulation, which might be contributing for protein's functionality and flexibility regions, we have calculated the averaged RMSF analysis of all the residues during the MD simulated time. From the comparative graphs (figure 7), it can be inferred that majorly fluctuating residues are present at 1100-1150 numbered residues. These residues were found to be fluctuating well below 3 Å for apo protein; above 4 Å for protein in complex with AAZ and around 3.5 Å for protein in complex with Quercetin compound, which signifies that this part of the protein in specific might be playing a crucial role for stronger ligand binding to the protein.

Hydrogen bonds are the main contributors for the overall stability of the protein structures along with other non-bonded forces. More the total number of hydrogen bonds, higher will be the rigidity of the protein, which might result in reduced activity of the protein. When the total number of intra molecular Hydrogen bonds present in the protein VEGFR2 in its apo form; in complex with AAZ and in complex with Quercetin was analyzed (table 2), it was revealed that protein structure was highly rigid in its apo state with an average of 120 intra molecular hydrogen bonds in a range of 105 to 145; As the simulation progresses, the graph (figure 8) evidenced that the overall intra molecular hydrogen bonds present in the protein are depleting from an average of 130 at initial time to 115 at the end of the simulation, which suggests that the protein is becoming flexible resulting for its activity. When intra molecular hydrogen bonds were analyzed in presence of AAZ compound, it was found to be maintaining an average of 80 with a range of 65 to 95, which shows that the protein has become flexible in presence of this compound leaving scope for its activity. When the intra molecular hydrogen bonds were analyzed for protein in presence of Quercetin compound, it was found to be maintaining an average of 125 in a range of 105 to 140, which depicts its strong inhibiting capability of this compound by make it further rigid to lessen its activity.

To further understand the contributions involved for the protein stability, we have monitored total Secondary structure elements (SSE) present in the protein like alpha helices and beta strands throughout the simulation trajectory. From the analysis it was revealed that the protein VEGFR2 maintaining about 36-42% of SSE composition of helices and strands over simulated time with an average of 39% in its apo state (Figure 9a); 32 to 44% with an average of 40% in complex with AAZ (Figure 9b) and 39-45% with an average of 42% in complex with Quercetin compound (Figure 9c). This SSE results further substantiates that protein in Quercetin is higher stable comparatively.

In order to visualize the conformation change behavior of VEGFR2 in presence of the ligands AAZ and Quercetin, we have superimposed the first (Pre MD) and last frames (Post MD) of the MD generated trajectory structures, it is observed that the protein structure has slightly expanded, and the minor movements responsible for this expansion have been observed with helices and loops in specific as shown in figure 10. As simulation progresses we have observed that the compounds AAZ and Quercetin are showing a flip of around 90^0 at the catalytic active site of VEGFR2 for its stabilization; further depicting the compound compatibility to the conformational changes at the VEGFR2's active site.

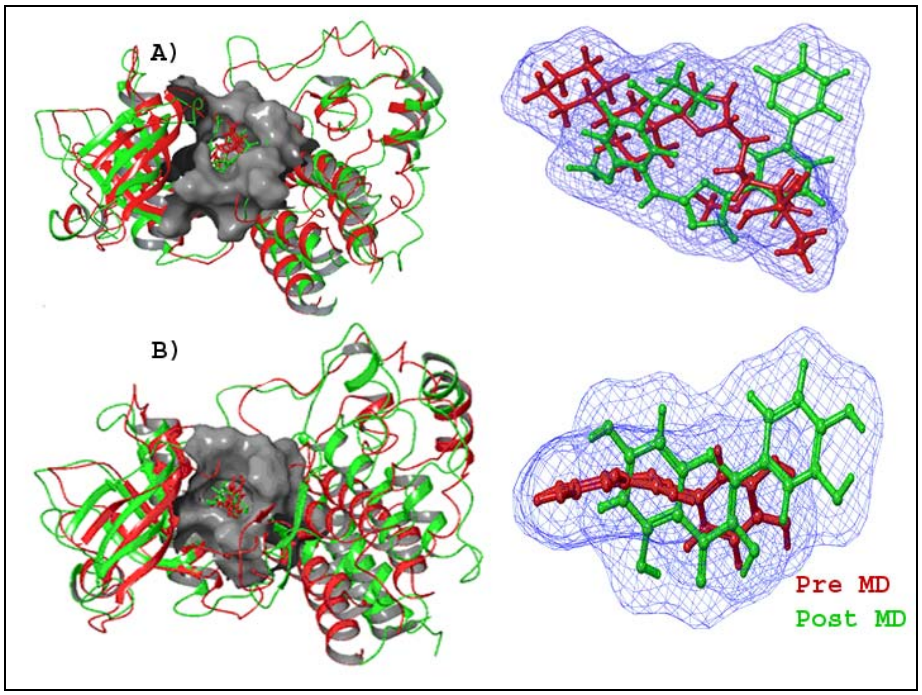

Fig 10: Superimposition of Pre MD and Post MD simulated VEGFR2 protein in complex with A) AAZ and B) Quercetin.

5.3 Interaction profile of AAZ and Quercetin with VEGFR2 during MD simulations

We have used Simulation interactions diagram protocol integrated within Desmond module for studying the detailed inter-molecular interactions involved in the receptor-ligand complex during MD simulations. A total of 3 (for AAZ) and 4 (for Quercetin) hydrogen bonds were observed with VEGFR2, frequent direct h-bonds were observed with residues CYS917; LEU1033 and CYS 1043 with around 80% occupancy during MD trajectory analysis for AAZ compound, these residues are also found to be participating in water bridges and hydrophobic contacts, apart from above mentioned direct hydrogen bonds forming residues, AAZ was found to be forming various other interactions like ionic interactions; water bridges and hydrophobic contacts with residues LEU838; VAL 846; GLU848; ALA 864; VAL 897; PHE 916; LYS 918; PHE 919; LEU 1017; ASN 1031; LYN 1041 and PHE1045 residues as shown in below figure 11**.**

When the interaction profile of Quercetin was observed, LYS866; GLU883; LYN1041 and ASH1044 residues were found to be forming direct hydrogen bonds with Quercetin compound within a range of 40 to 100% occupancy during MD trajectory. Among the hydrogen bonds forming residues, LYS866; LYN 1041 and ASH1044 residues were also found to be forming water bridges. Apart from above mentioned direct hydrogen bonds forming residues, AAZ was found to be forming various other interactions like ionic interactions; water bridges and hydrophobic contacts with LEU 838; ARG 840; GLY 841; ALA 842; VAL 846; ILE 847; GLU 848; ALA 864; VAL 897; VAL 914; PHE 916; CYS 917; LYS 918; PHE 1016; LEU 1017; HIS 1024; ILE 1042; CYS 1043; PHE 1045 and LEU 1047 residues as shown in below figure 12**.**

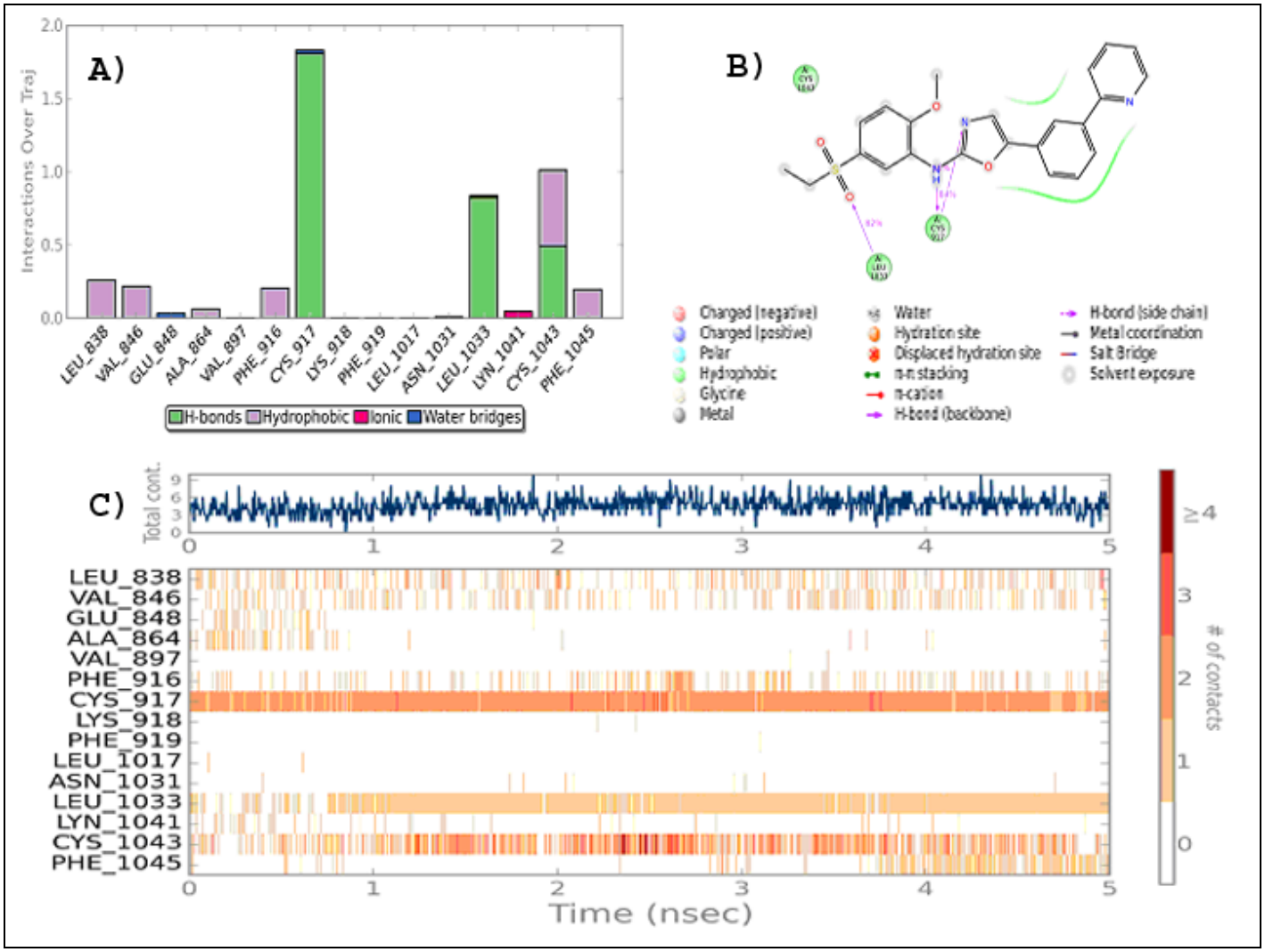

Fig 11: A) Analysis of various interactions involved in stabilizing VEGFR2-AAZ complex. **B)** Analysis of percentage occupancy of the direct hydrogen bonds formed between AAZ and VEGFR2 residues. **C)** Analysis of total contacts formed between VEGFR2 residues and AAZ during MD simulation.

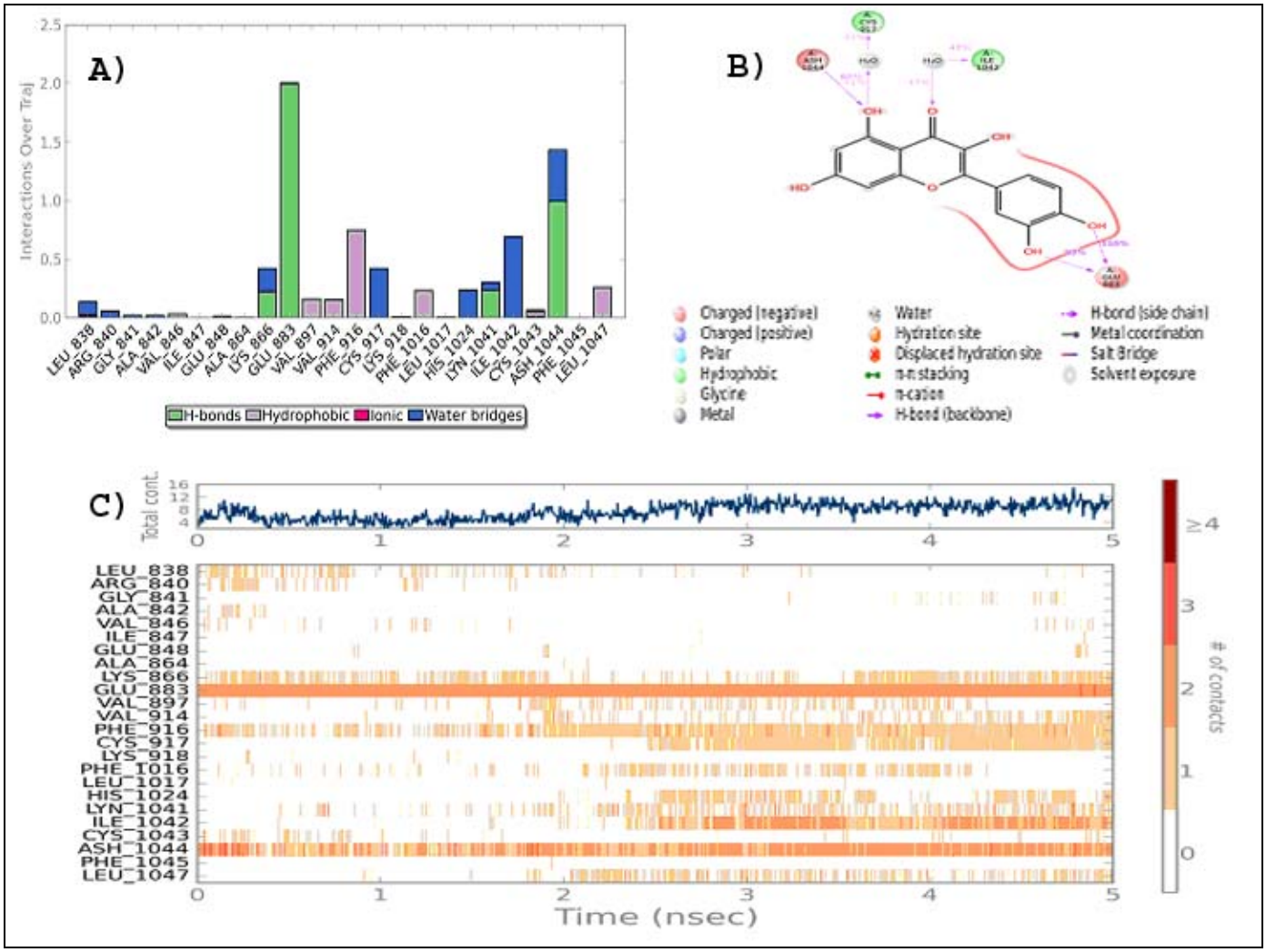

Fig 12: A) Analysis of various interactions involved in stabilizing VEGFR2-Quercetin complex. **B)** Analysis of percentage occupancy of the direct hydrogen bonds formed between QUERCETIN and VEGFR2 residues. **C)** Analysis of total contacts formed between VEGFR2 residues and QUERCETIN during MD simulation.

To examine and estimate the ligand conformational evolution of every rotatable bond (RB) in the ligand throughout the simulation trajectory facilitating for their stabilized conformation, we have analyzed the torsional degree of freedom for the rotatable bonds present in the ligand. Each rotatable bond torsion is accompanied by a color-coded dial plot and bar plots of the same color. Conformation of the torsion is described by Dial (or radial) plots. Center of the radial plot represents the beginning of the simulation and the time evolution is plotted radially outwards. The probability density of the torsion is summarized by the bars on the dial plots. Potential energy consumed for that particular conformation is expressed in *kcal/mol* on the left *Y*-axis of the chart. For the compound AAZ, a total of 7 rotatable bonds were observed with various degrees of freedom as shown in figure 13a by utilizing a total of 47.67 kcal/mol of energy. For the compound Quercetin, a total of five rotatable bonds were observed with various degrees of freedom as shown in figure 13b by utilizing a total of 28.04 kcal/mol of energy.

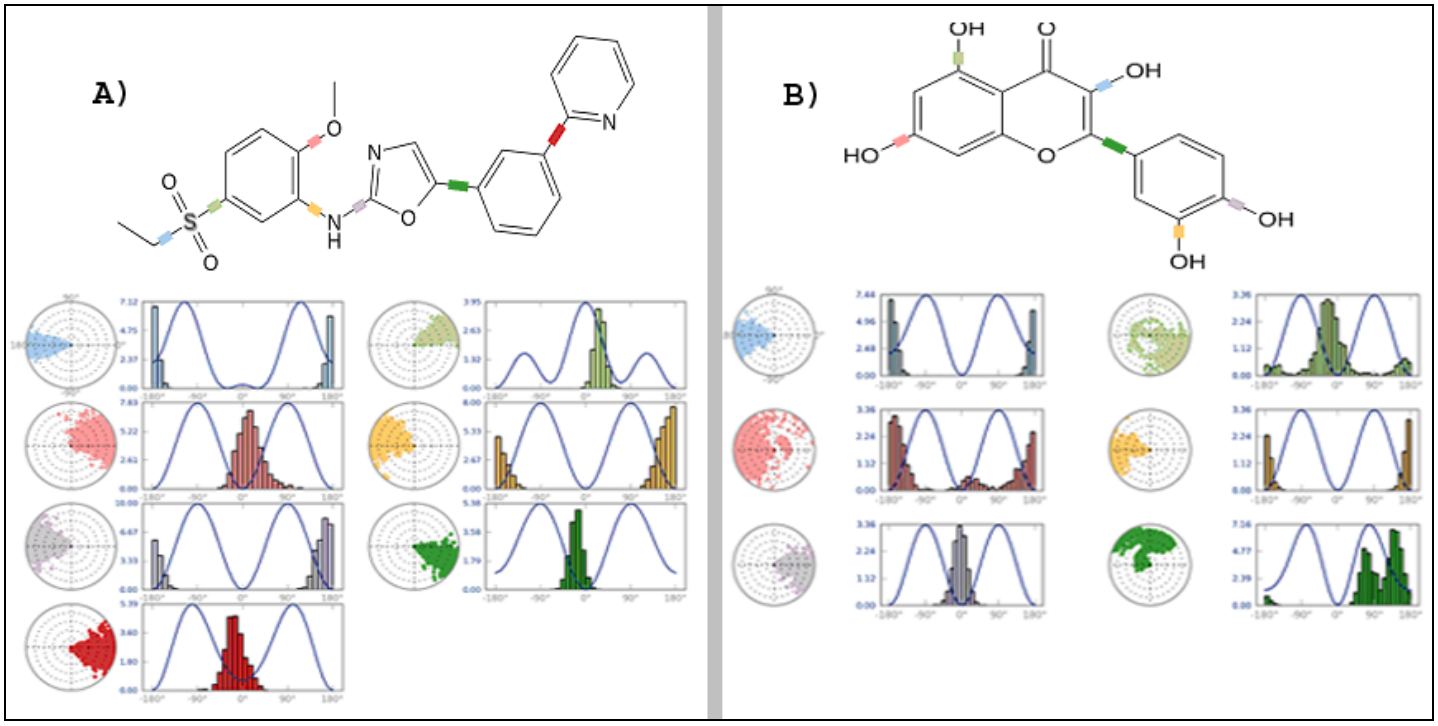

Fig 13: Analysis of torsional degree of freedom during MD simulation trajectory for the rotatable bonds present in the A) AAZ and B) Quercetin compounds.

6. Conclusion

The present study demonstrated that VEGFR2 is a target of Quercetin and provided mechanistic insights for the ability of naturally occurring Quercetin as a valuable small ligand molecule for cancer treatment via anti-angiogenesis targeting VEGFR2. Results from *de novo* molecular dynamic simulations for 5 ns showed that the trajectories of the protein complexed with ligand Quercetin was stable over a considerably long time period of 5 ns, with the energies of the complex being lowered in comparison to the un-docked protein and in complex with AAZ consolidating the thermodynamic stability and substantiates the hypothesis that Quercetin has the potential to inhibit VEGFR2. Furthermore, ligand interactions revealed during docking and molecular dynamic simulations with catalytically important residues could be critical for its inhibitory potential. The present knowledge is of high value for computational screening of VEGFR2 drugs towards further enhancing the discovery of VEGFR2 target specific drug compounds by understanding the molecular interaction basis between ligand and receptor.

7. Acknowledgement

Syed Hussain Basha great fully acknowledge the much need help of Raghu Rangaswamy, Anirban Banerjee and Vinod Devaraji towards providing us with Schrodinger software. Prakash Bethapudi would like to sincerely thank his guide Professor Sreenivasa Reddy E, for his constant support and encouragement in carrying out this research work.

8. Authors' contribution

Conceived and designed the experiments: SHB, MR. Performed the experiments: SHB, PB, MR, NVSVMM. Analysis and drafting of the paper: SHB, MR and FA. Editing of the paper: SRE, FA. All the authors have read and approved the manuscript.

9. Competing interests

The authors declare that they have no competing interests.

10. Supplementary material 1: ADME parameters of AAZ and Quercetin compounds generated using Qikprop module of Schrodinger.

11. References

1. "How many different types of cancer are there?: Cancer Research UK : Cancer Help UK". Available http://www.cancerresearchuk.org/cancer-help/about-cancer/cancer-questions/how-many-different-types-of-cancer-are-there. 2014.
2. American cancer society. Hodgkin disease detailed guide. Atlanta, Ga: American cancer society, 2012, 1-54.
3. International agency for research on cancer .World cancer factsheet (2012), Cancer research UK. Available http://globocan.iarc.fr/Pages/fact_sheets_cancer.aspx. Accessed, 2014.
4. Angiogenesis. New York, whiteplains. The leukemia and lymphoma society, Available www.lls.org Accessed, 2014.
5. Rahmi Oklu, Thomas G, Walker MD, Stephan Wicky, Robin Hesketh *et al.* Angiogenesis and current anti angiogenic strategies for the treatment of cancer. Journal of vascular and interventional radiology 2010; 21:1791-1805.
6. Ann Hoeben, Bart Landuyt, Martins S Highley, Hans Wildiers, Allan T, Van Oosterom *et al.* Vascular endothelial growth factor and angiogenesis. Pharmacological reviews 2004; 56(4):549-580.
7. H Bernard, B Grammy susini, N Ainaoui, L Van Den Berghe, A Peurichard, S Javerzat *et al.* The p53 isoform Δ133p53α, stimulates angiogenesis and tumor progression, oncogene, 2012, 1-11.
8. Peter carmeliet. Angiogenesis in health and disease state. Nature medicine 2003; 9:653-660.

9. Yang JC, Haworth L, Sherry RM, Hwu P, Schwartzentruber DJ, Topalian SL *et al.* A randomized trial of bevacizumab, an anti-vascular endothelial growth factor antibody, for metastatic renal cancer. N Engl J Med 2003; 349:427e434.
10. Brekken RA, Thorpe PE. Vascular endothelial growth factor and vascular targeting of solid tumors. Anticancer Res 2001; 21:4221–4229.
11. Michael Yakes F, Jason Chen, Jenny Tan. Cabozantinib (XL184). A Novel MET and VEGFR2 Inhibitor, Simultaneously Suppresses Metastasis, Angiogenesis, and Tumor, Growth. American Association for Cancer Research 2011; 10(12):2298- 2309.
12. Miroslav Murár1, Gabriela Addová, Andrej Bohac. Synthesis of 5-(ethylsulfonyl)-2-methoxyaniline: An important pharmacological fragment of VEGFR2 and other inhibitors. Beilstein J Org Chem 2013; 9:173–179.
13. Verma S, Singh A, Mishra A. Taxifolin acts as type I inhibitor for VEGFR-2 kinase: Stability evaluation by molecular dynamic simulation. Journal of Applied Pharmaceutical Science 2013; 02(01):41-46.
14. Jeong Hun Kim, Jin Hyoung Kim, You Mie Lee, Eun-Mi Ahn Kyu-Won Kim *et al.* Decursin inhibits retinal neovascularization via suppression of VEGFR-2 activation, Molecular Vision, 2009; 15:1868-1875.
15. Kan V Lu, Jeffrey P Chang, Christine A Parachoniak, Melissa M Pandika, Manish K Aghi *et al.* VEGF Inhibits Tumor Cell Invasion and Mesenchymal Transition through a MET/VEGFR2 Complex. Cancer Cell 2012; 22:21–35.
16. Dellinger MT, Brekken RA. Phosphorylation of Akt and ERK1/2 is required for VEGF-A/VEGFR2-induced proliferation and migration of lymphatic endothelium. PloS one 2011; 6(12):e28947.
17. Kyungik Lee a,b, Ki-Woong Jeong c, Yeonjoo Lee b, Ji Yeon Song b, Maeng Sup Kim b, Gwan Sun Lee b, Yangmee Kim c. Pharmacophore modeling and virtual screening studies for new VEGFR-2 kinase inhibitors. European Journal of Medicinal Chemistry 2010; 45:5420e5427
18. Christian Peifer a, Stefanie Bu¨hler a, Dominik Hauser a, Katrin Kinkel a, Frank Totzke b, Christoph Scha¨chtele b *et al.* Design, synthesis and characterization of N9/N7-substituted 6-aminopurines as VEGF-R and EGF-R inhibitors. European Journal of Medicinal Chemistry 2009; 44:1788e1793
19. Hertog MGL, Hollman PCH, Katan MB. Content of potentially anticarcinogenic flavonoids of 28 vegetables and 9 fruits commonly consumed in The Netherlands. Journal of Agricultural and Food Chemistry 1992; 40:2379–2383.
20. Bischoff SC. Quercetin: potentials in the prevention and therapy of disease. Current Opinion in Clinical Nutrition & Metabolic Care 2008; 11:733.
21. Murakami A, Ashida H, Terao J. Multitargeted cancer prevention by quercetin. Cancer letters 2008; 269:315–325.
22. Basha *et al.* Computational repositioning of ethno medicine elucidated gB-gH-gL complex as novel anti herpes drug target. BMC Complementary and Alternative Medicine 2013; 13:85.
23. Kumar P *et al*. Quercetin inhibits angiogenesis mediated human prostate tumor growth by targeting VEGFR-2 regulated AKT/mTOR/ P70S6K Signaling Pathways. Public library of science, 2012; 7(10):1-10
24. Harris PA, Cheung M, Hunter RN, Brown ML, Veal JM, Nolte RT *et al.* Discovery and evaluation of 2-anilino-5-aryloxazoles as a novel class of VEGFR2 kinase inhibitors. Journal of medicinal chemistry 2005; 48(5):1610-1619.
25. Bernstein FC, Koetzle TF, Williams GJ, Meyer Jr EE, Brice MD, Rodgers JR *et al.* The Protein Data Bank: A Computer-based Archival File for Macromolecular Structures. J of Mol Biol 1977; 112:535.
26. Small-Molecule Drug Discovery Suite 2013-3: Glide, version 6.1, Schrödinger, LLC, New York, NY, 2013.
27. ö Friesner RA, Murphy RB, Repasky MP, Frye LL, Greenwood JR, Halgren TA *et al.* Extra Precision Glide: Docking and Scoring Incorporating a Model of Hydrophobic Enclosure for Protein-Ligand Complexes. J Med Chem 2006; 49:6177–6196.
28. ö Halgren TA, Murphy RB, Friesner RA, Beard HS, Frye LL, Pollard WT *et al.* Glide: A New Approach for Rapid, Accurate Docking and Scoring. 2. Enrichment Factors in Database Screening. J Med Chem 2004; 47: 1750–1759.
29. ö Friesner RA, Banks JL, Murphy RB, Halgren TA, Klicic JJ, Mainz DT *et al.* Glide: A New Approach for Rapid, Accurate Docking and Scoring. 1. Method and Assessment of Docking Accuracy. J Med Chem 2004; 47:1739–1749.
30. Schrödinger Release 2013-3: Maestro, version 9.6, Schrödinger, LLC, New York, NY, 2013.
31. Schrödinger Release 2013-3: Schrödinger Suite 2013 Protein Preparation Wizard; Epik version 2.6, Schrödinger, LLC, New York, NY, 2013; Impact version 6.1, Schrödinger, LLC, New York, NY, 2013; Prime version 3.3, Schrödinger, LLC, New York, NY, 2013.
32. ö Sastry GM, Adzhigirey M, Day T, Annabhimoju R, Sherman W. Protein and ligand preparation: parameters, protocols, and influence on virtual screening enrichments. J Comput Aid Mol Des 2013; 27(3):221-234.
33. Jorgensen WL, Maxwell DS, Tirado-Rives J. Development and testing of the OPLS all-tom force field on conformational energetics and properties of organic liquids. J Am Chem Soc 1996; 118:11225–11236.
34. Kaminski G, Friesner RA, Tirado-Rives J, Jorgensen W L. Evaluation and reparameterization of the OPLS-AA force field for proteins via comparison with accurate quantum chemical calculations on peptides. J Phys Chem B 2001; 105:6474–6487.
35. Schrödinger Release 2013-3: LigPrep, version 2.8, Schrödinger, LLC, New York, NY, 2013.
36. Small-Molecule Drug Discovery Suite 2013-3: QikProp, version 3.8, Schrödinger, LLC, New York, NY, 2013.
37. Lipinski CA, Lombardo F, Dominy BW, Feeney PJ. Experimental and computational approAChEs to estimate solubility and permeability in drug discovery and development settings. Advanced Drug Delivery Reviews 1997; 23:3-25.
38. Lyne PD, Lamb ML, Saeh JC. Accurate prediction of the relative potencies of members of a series of kinase inhibitors using molecular docking and MM-GBSA scoring. J Med Chem 2006; 49:4805–4808.
39. Das Koh Y, Tojo Y, Ghosh AK, Mitsuya H. Prediction of potency of protease inhibitors using free energy

simulations with polarizable quantum mechanics-based ligand charges and a hybrid water model. J Chem Inf Model 2009; 49:2851–2862.
40. Schrödinger Release 2013-3: Desmond Molecular Dynamics System, version 3.6, D. E. Shaw Research, New York, NY, 2013. Maestro-Desmond Interoperability Tools, version 3.6, Schrödinger, New York, NY, 2013.
41. ö Shivakumar D, Williams J, Wu Y, Damm W, Shelley J, Sherman W. Prediction of Absolute Solvation Free Energies using Molecular Dynamics Free Energy Perturbation and the OPLS Force Field. J Chem Theory Comput 2010; 6:1509–1519.
42. Kevin J Bowers, Edmond Chow, Huafeng Xu, Ron O Dror, Michael P Eastwood, Brent A Gregersen *et al.* Scalable Algorithms for Molecular Dynamics Simulations on Commodity Clusters. *Proceedings of the ACM/IEEE Conference on Supercomputing (SC06), Tampa, Florida*, 2006.
43. Jorgensen WL, Chandrasekhar J, Madura JD, Impey RW, Klein ML. Comparison of simple potential functions for simulating liquid water. J Chem Phys 1983; 79:926-935.
44. Shinoda, Wataru, Masuhiro Mikami. Rigid-body dynamics in the isothermal-isobaric ensemble: A test on the accuracy and computational efficiency. Journal of computational chemistry 2003; 24(8):920-930.
45. Nosé, Shuichi. A unified formulation of the constant temperature molecular dynamics methods. The Journal of Chemical Physics 1984; 81:511.
46. Warren GL, Andrews CW, Capelli AM, Clarke B, LaLonde J, Lambert MH *et al.* A critical assessment of docking programs and scoring functions. J Med Chem 2006; 49(20):5912-5931.